uninflatable encodes a novel ectodermal apical surface protein required for tracheal inflation in *Drosophila*

Liang Zhang and Robert E. Ward IV[1]

Department of Molecular Biosciences, University of Kansas, Lawrence, Kansas 66045

Running head: *uninflatable* in tracheal development

[1]Corresponding author: Robert E. Ward IV, Department of Molecular Biosciences, University of Kansas, 1200 Sunnyside Ave., Lawrence, Kansas 66045

E-mail: robward@ku.edu

Phone: (785) 864-5235

Fax: (785) 864-5294

Abstract

The tracheal system of *Drosophila melanogaster* has proven to be an excellent model system for studying the development of branched tubular organs. Mechanisms regulating the patterning and initial maturation of the tracheal system have been largely worked out, yet important questions remain regarding how the mature tubes inflate with air at the end of embryogenesis, and how the tracheal system grows in response to the oxygen needs of a developing larva that increases nearly 1000-fold in volume over a four day period. Here we describe the cloning and characterization of *uninflatable* (*uif*), a gene that encodes a large transmembrane protein containing carbohydrate binding and cell signaling motifs in its extracellular domain. Uif is highly conserved in insect species, but does not appear to have a true ortholog in vertebrate species. *uif* is expressed zygotically beginning in stage 5 embryos, and Uif protein localizes to the apical plasma membrane in all ectodermally derived epithelia, most notably in the tracheal system. *uif* mutant animals show defects in tracheal inflation at the end of embryogenesis, and die primarily as larvae. Tracheal tubes in mutant larvae are often crushed or twisted, although tracheal patterning and maturation appear normal during embryogenesis. *uif* mutants larvae also show defects in tracheal growth and molting of their tracheal cuticle.

Key words: *Drosophila*; trachea; cuticle; tube size control; air filling; molting; *CG9138*; *SP1070*

Introduction

Organs composed of networks of branched tubes play essential roles in the transport of liquids and gasses in all animals. Examples include the kidney, lung and vascular system of mammals and the tracheal system of insects. In general these organs are well-ordered structures with stereotypic developmental patterns. Maturation of these organs during development yields tubes of appropriate caliber to support the fluid or gas movement throughout the organ. Continued growth of these organs after birth is also critical to support the needs of a rapidly growing animal, as postnatal hypotrophy of organs including the lung and kidney can be pathological (Kerecuk et al., 2008; Shi et al., 2007).

The larval tracheal system of *Drosophila melanogaster* is an excellent model, not only for the stereotypic patterning of a branched tubular organ, but also for its maturation into a functional organ and its ability to expand in size and complexity as the animal grows. Over the past decade genetic and cell biological approaches have provided extensive knowledge regarding the mechanisms involved in the patterning of the tracheal metameres and how adjacent metameres fuse to form a complete tracheal system (recently reviewed in Affolter and Caussinus, 2008). In recent years the mechanisms required for final maturation of the tracheal tubes have also started to come into focus. Tracheal maturation is a multistep process necessary to produce tracheal tubes of appropriate length and diameter to effectively deliver air to the peripheral tissues while sustaining an inflated state. Steps in this process include the secretion of chitinous extracellular matrix into the lumen of the newly formed tracheal system, and the eventual clearance of lumenal protein to leave liquid filled tracheal tubes. The first step in this process requires a chitin synthase encoded by the gene *krotzkopf verkehrt* (*kkv*) and an UDP-*N*-acetylglucosamine diphosphorylase encoded by the *mummy* (*mmy*) gene to produce a chitinous matrix in the lumen of stage 14 embryos (Araujo et al., 2005; Devine et

al., 2005; Tonning et al., 2005). This early phase of tube maturation also requires the small GTPase encoded by *sar1* that regulates vesicle traffic from the endoplasmic reticulum to the Golgi apparatus (Tsarouhas et al., 2007), and thereby controls the secretion of key matrix proteins. Together these proteins regulate the dilation of the tracheal lumen to adopt the appropriate diameter. Subsequently, the secretion of a pair of putative chitin deacetylase enzymes encoded by *serpentine* (*serp*) and *vermiform* (*verm*) regulates the size of the apical surface of the tracheal cells, and thereby controls tracheal length, through an unknown mechanism (Luschnig et al., 2006; Wang et al., 2006). Interestingly, mutations in genes encoding components of the septate junction, a lateral membrane domain analogous to the vertebrate tight junction in its paracellular barrier function, also result in tracheal length defects likely through a requirement for intact septate junctions in the proper secretion of Serp and Verm (and possibly other proteins) into the tracheal lumen (Behr et al., 2003; Llimargas et al., 2004; Paul et al., 2003; Wang et al., 2006; Wu and Beitel, 2004; Wu et al., 2007). Later, during stage 17 of embryogenesis, the modified chitin and other luminal proteins are cleared through a process that requires clathrin-mediated endocytosis, rab5, and a transmembrane protein encoded by *wurst* that appears to regulate tracheal endocytosis through its cytoplasmic clathrin binding motifs and a J-domain that binds to the chaperone Hsc70-4 (Behr et al., 2007; Tsarouhas et al., 2007).

The final stages of tracheal maturation including the organization of the tracheal cuticle and subsequent air filling are less well understood. When the chitinous material is being secreted into the tracheal lumen in preparation for tube dilation, the tracheal cells also begin to secrete proteins into the apical extracellular matrix that eventually assembles into a characteristic cuticle containing densely packed parallel rows of cuticular ridges called taenidia. This cuticle provides an important barrier to dehydration and infection while the taenidial organization provides mechanical stability to the tubes. This mechanical role of the taenidia is best demonstrated by mutations in the formin

homology gene *daam*. *daam* encodes an actin polymerizing protein, and mutations in *daam* affect a subapical actin cytoskeleton that forms circumferential rings in register with the taenidial ridges. *daam* mutations result in disorganized taenidia and collapsed tracheal tubes (Matusek et al., 2006). At the end of embryogenesis, the tracheal lumen is cleared of fluid and inflated with air via a mechanism that is still unclear, yet likely requires the action of epithelial sodium channels (Liu et al., 2003).

During larval stages, the tracheal system continues to grow to meet the oxygen needs of the developing larvae. Beitel and Krasnow (2000) observed that tracheal length increases gradually throughout larval development, whereas tracheal diameter increases in a saltatory fashion coupled to the tracheal molts. Since there is no cell proliferation in the larval trachea, these changes result from growth of the tracheal cells that must somehow be coupled to the growth of the larva. The mechanisms involved in this process have yet to be elucidated, as all of the tube size control genes that have been characterized affect embryonic development rather than larval tracheal growth.

Here we describe the cloning and initial characterization of *uninflatable* (*uif*), a novel gene that encodes an apically localized transmembrane protein expressed at high levels in the developing tracheal system. The large extracellular domain of Uif contains several different carbohydrate binding domains and epidermal growth factor repeats, whereas the short cytoplasmic domain is devoid of conserved domains. Uif is highly conserved in insect species. Zygotic loss of *uif* results in defects in tracheal inflation during late embryogenesis without obviously affecting tracheal patterning or maturation prior to air filling. In addition, *uif* mutant larvae display a tracheal growth defect and fail to effectively molt their tracheal cuticle.

Materials and methods

Drosophila strains

The *uif*^{1} allele is an EMS induced second-site mutation on the *E(br)155* chromosome reported in Ward et al., (2003). *uif*^{2B7} and *uif*^{1A15} were isolated in an F_2 EMS mutagenesis screen described below. *UAS-CG9138RNAi* strains (v1047 and v1050; hereafter referred to as *UAS-uifRNAi*) were obtained from the Vienna *Drosophila* RNAi Center (VDRC, Vienna, Austria; Dietzl et al., 2007). *Df(2L)Exel7029*, *breathless* (*btl*)-*Gal4*, *daughterless* (*da*)-*Gal4*, *engrailed* (*en*)-*Gal4*, *yw ; Bl L / CyO, P{w*$^{+}$*, hs-hid}* and *w*^{1118} were obtained from the Bloomington *Drosophila* Stock Center (Bloomington, IN). *w*^{1118} was used as the wild type strain for the experiments reported here. *uif*^{1}, *uif*^{2B7}, and *uif*^{1A15} were balanced with *CyO, P{w*$^{+}$*, Dfd-EYFP}* (Le et al., 2006). All *Drosophila* stocks were maintained on media consisting of corn meal, sugar, yeast, and agar in incubators maintained at a constant temperature of 21°C or in a room that typically fluctuated between 21°C and 22.5°C. Genetic experiments were conducted in incubators controlled at a constant temperature of 25ºC.

EMS Mutagenesis and screening

Two cohorts of approximately thirty 3-5 day old *w*^{1118} males were treated with 25 mM methanesulfonic acid ethyl ester (EMS) in empty plastic vials for approximately 16 hours. Each cohort was mated to approximately thirty *yw ; Bl L / Cyo, P{w*$^{+}$*, hs-hid}* virgin females in bottles maintained at 21°C. The adults were transferred to fresh bottles after 3 days and subsequently transferred once more after an additional 2 days. Single balanced male progeny (*yw / Y ; * / Cyo, P{w*$^{+}$*, hs-hid}*) were crossed to 5-6 *w ; uif*^{1} *Cyo, P{w*$^{+}$*, Act-GFP}* virgin females in narrow short vials. All single male cross vials were heat shocked in a 37°C water bath for one hour on days 5 and

6 after setting the cross to eliminate any flies bearing the *hs-hid* balancer chromosome. We established balanced stocks by sibling mating of all the vials that produced only * / *Cyo, P{w$^+$, Act-GFP}* offspring. Two of the lines (referred to as 1A15 and 2B7) also failed to complement *Df(2L)Exel7029* (cytological breakpoints 27C4;27D4), suggesting that they were new *uif* alleles. Sequencing of genomic DNA isolated from homozygous mutant late embryos (by the DNA Facility of the Iowa State University Office of Biotechnology in Ames, IA) confirmed this notion. All exonic sequences and intron/exon boundaries were sequenced on one strand of the genomic DNA. Regions containing putative mutations were verified by sequencing both strands. Specifically, both strands representing nucleotides 27207-28780 of GenBank sequence **AAC008326** were sequenced for *uif^1*, as were nucleotides 29856-31290 for *uif^{2B7}* and *uif^{1A15}*.

Genomic organization determination and phylogenetic analyses

Total RNA was collected from 12-24 hour *w^{1118}* embryos and late third instar larval wing imaginal discs. cDNAs were generated using SuperScript III reverse transcriptase (Invitrogen, Carlsbad, CA). DNA primers corresponding to sequences spanning predicted exon/intron boundaries were used for PCR, and the resulting products were examined for predicted sizes by gel electrophoresis. Three independent primer sets spanning exon 10 and 11 produced double bands differing by ~100 bp in both the embryonic and imaginal disc cDNA collections. These DNA fragments were recovered and sequenced at the Iowa State University DNA facility. For the phylogenetic analysis, the cytoplasmic domain of Uif (NH2-

WMICVRSTKRRDPKKMLTPAIDQTGSQVNFYYGAHTPYAESIAPSHHSTYAHYYDDEEDG

WEMPNFYNETYMKDGLHGGKMSTLARSNASLYGTKEDLYDRLKRHAYTGKKEKSDSDS

EVQ-COOH) was BLASTed against the nonredundant protein sequence database and the following 19 sequences were identified as showing significant sequence similarity to Uif throughout the entire

protein sequence: XP_002067066.1, AAF63500.1, XP_001357402.2, XP_002088091.1, XP_001988186.1, XP_001970107.1, XP_001961405.1, XP_002002737.1, XP_002078458.1, XP_002018755.1, XP_002051404.1, XP_001861365.1, XP_001606223.1, XP_001658862.1, XP_974965.2, EEB13939.1, XP_396277.3, XP_001949468.1, XP_312182.4. Notably, the cytoplasmic domain of Uif was not found outside the insect order, and all sequences showing similarity to the cytoplasmic domain contained a full-length Uif protein. These sequences were then aligned using MUSCLE (Multiple sequence comparison by log-expectation; Edgar, 2004). For simplicity sake in drawing the tree shown in Fig. 1B, we eliminated *D. virilis*, *D. persimilis*, *D. similans*, and *D. erecta*, which all mapped within the *Drosophila* subgroup. A pairwise comparison between *D. melanogaster* and *Acythosiphon pisum* was conducted using BLAST2seq on the NCBI server.

Lethal phase and phenotypic analyses

Prior to conducting lethal phase and terminal phenotypic analyses on *uif* mutants, we cleaned the uif^{1A15} and uif^{2B7} mutant chromosomes by sequentially recombining *P*- or *PiggyBac* elements onto and off of the *uif* chromosomes. For the centromere proximal side we used $P\{XP\}CG6739^{d09967}$ (in 28B4), and for the centromere distal side we used $PBac[PB]stai^{c01639}$ (in 26B7). Since we were unable to recombine uif^{1} apart from the *E(br)155* mutation, we have not included this allele in the analyses described here. uif^{1A15}, uif^{2B7}, and *Df(2L)Exel7029* were balanced with *CyO, P{*w^{+}*, Dfd-EYFP}* such that mutant embryos and larvae could be unambiguously identified by the absence of YFP. Embryonic staging was determined by gut morphology. RNAi experiments were performed by crossing *UAS-uifRNAi* strains (v1047 and v1050) to *btl-Gal4*, *da-Gal4* or *en-Gal4* strains. It should be noted that *btl-Gal4, UAS-GFP* homozygous embryos showed greater than 40% tracheal inflation defects, but when outcrossed to w^{1118}, the *btl-Gal4, UAS-GFP/+* embryos showed no

tracheal inflation defects. Embryonic lethality was determined as the percentage of unhatched embryos 48 hours after selecting non-YFP-expressing mutant embryos produced through a four-hour egg collection. Larval lethality was determined as the percentage of non-pupariating mutant larvae seven days after selecting newly hatched mutant larvae. All experiments were performed in triplicate and means with standard deviations were determined. Non-hatched embryos were dechorionated in 6% sodium hypochloride, mounted on microscope slides in Hoyer's medium and subsequently examined for cuticular phenotypes on a Nikon Eclipse 80*i* compound microscope. Similarly, mutant larvae from parallel experiments were examined for defects on Zeiss SV6 or Leica MZ7.5 stereomicroscopes and mounted in Halocarbon oil 700 (Sigma, St. Louis, MO). The non-molted larva shown in Fig. 5E was mounted in Hoyer's medium. Wild type and *uif* mutant larval tracheae were hand-dissected from appropriately staged animals in PBS and mounted in 90% glycerol, 100 mM Tris, pH 8.0. Larval staging was determined by anterior spiracle morphology, although mouthpart morphology was additionally used to confirm the stage of five-day-old uif^{2B7} second instar larvae. All cuticular phenotypes were documented on a Nikon Eclipse 80*i* compound microscope equipped with a Photometrics CoolSNAP *ES* high performance digital CCD camera. Photomicrographs were adjusted for brightness and contrast with the Adobe Photoshop (version CS3, San Jose, CA), and figures were compiled in Adobe Illustrator (version CS3, San Jose, CA).

Time-lapse movies were generated by mounting stage 17 uif^{2B7} mutant embryos on apple juice plates, and automatically collecting brightfield images every minute for 230 minutes using MetaMorph (Molecular Devices, Sunnyvale, CA) software on a Nikon Eclipse 80*i* compound microscope equipped with a Photometrics CoolSNAP *ES* high performance digital CCD camera using a 4X Nikon Plan Apo lens. The image stack was opened in ImageJ (Rasband, 1997-2009) and saved as image sequences that were then changed to 8-bit images and adjusted for brightness and contrast in Adobe Photoshop. These adjusted images were then opened in ImageJ, cropped and

saved as an AVI file with a rate of 4 frames per second. We subsequently cropped the image sequence files to visualize one embryo using ImageJ, and selected individual frames that were compiled in Adobe Illustrator to make Fig. 3.

To quantify the tracheal length defects in *uif* mutant third instar larvae, we collected newly hatched w^{1118}, uif^{2B7}, uif^{dA15}, and *btl-Gal4/UAS-uifRNAi* larvae and grew them on separate apple juice plates at 25ºC until they were either second or third instar larvae (as judged by anterior spiracles). Individual live larvae were then mounted in halocarbon oil on microscope slides with cover slips. After approximately 5 minutes, brightfield photomicrographs were taken on a Nikon Eclipse 80*i* compound microscope equipped with a Photometrics CoolSNAP *ES* high performance digital CCD camera using a 4X Nikon Plan Apo lens. Individual images were opened in MetaMorph and lines were drawn using multi-line to record the total body length or tracheal length. Pixel lengths were then obtained from the MetaMorph software using the region measurements tool. For tracheal length, we measured the distance along the dorsal trunk from the posterior spiracles to the transverse connective that originated in abdominal segment 4 during embryogenesis. It should be noted that in the *uif* mutant larvae, this TC was always physically located in more posterior segments, whereas this TC was almost always found in A4 in the w^{1118} larvae. For each larva, we determined the ratio of the partial tracheal length to full body length. We then determined the mean with standard deviation for each genotype.

RNA in situ hybridization

RNA *in situ* hybridization was performed as described in Choksi et al., (2006). A 646 nucleotide anti-sense probe for *uif* (corresponding to nucleotides 4216 to 4864 of GenBank sequence **AF239608**) was generated using a T7 DIG RNA labeling kit (Roche Applied Science, Indianapolis, IN). The template for anti-sense probe synthesis was generated by PCR amplification from a 12-24

hour embryo cDNA collection using the following primers: 5'-ACTGCGATGTCAATGCCTACTGC-3' and 5'-CAGTAATACGACTCACTATTACTACTG CACTTCGCTATCACTATCACTC-3' (T7 promoter sequence is underlined). A complementary sense probe was used as a control. The template for sense probe synthesis was generated by PCR amplification from a 12-24 hour embryo cDNA collection using the following primers: 5'-CAGTAATACGACTCACTATTAACTGCGATGTCAATGCCTACTGC-3' and 5'-CTACTGCACTTCGCTATCACTATCACTC-3 (T7 promoter sequence is underlined).

Generation of anti-Uif antibodies

To generate antiserum against Uif, nucleotides 2832 to 3659 of GenBank nucleotide sequence **AF239608** were cloned into a modified pET21a vector. This represents amino acids 2882-3157 of Uif, and its location is depicted in Fig. 1. The protein was overexpressed in *E.Coli* BL21 (DE3) cells, solubilized in binding buffer (20mM Tris-HCl pH8.0 500mM NaCl, 5mM Imidazole) with 6M urea, and purified through Ni^{2+} affinity chromatography. Purified protein was pooled and dialysis against PBS, in which it formed a precipitate. Purified precipitated protein was used for antibody generation in guinea pigs at the Pocono Rabbit Farm and Laboratory Inc. (PRF&L, Canadensis, PA). The guinea pig anti-Uif serum was subsequently affinity purified at PRF&L.

Immunostaining and dye exclusion experiments

Embryos were fixed and processed for antibody staining as described in Fehon et al., (1991). For larval expression studies, the larvae were torn in half, turned inside out and fixed at room temperature for 20 minutes in 4% paraformaldehyde in PBS. The following primary antibodies were used at the given dilutions: affinity purified guinea pig anti-Uninflatable 1:20, mouse anti-Crumbs 1:100 (clone Cq4 from the Developmental Studies Hybridoma Bank at the University of

Iowa, Iowa City, IA), mouse anti-Armadillo 1:100 (clone N27A1, DSHB), mouse anti-Dlg 1:100 (clone 4F3, DSHB), mouse anti-Fasiclin 3 1:300 (clone 7G10, DSHB), and mouse anti-Coracle 1:400 (gift from Richard Fehon, University of Chicago; Fehon et al., 1994). Secondary antibodies were obtained from Jackson ImmunoResearch Laboratories (West Grove, PA) and used at 1:400. Alexa Fluor 555 conjugated wheat germ agglutinin (WGA) was used at a concentration of 1μg/ml (Invitrogen, Carlsbad, CA). Rhodamine conjugated Chitin Binding Probe (CBP) was used at 1:500 according to the manufacturers recommendation (New England Biolabs Inc., Beverly, MA). Congo red staining was performed by incubating fixed embryos (ten minutes in 4% paraformaldehyde at room temperature) with a 1.5 μg/ml solution of Congo Red (Sigma, St. Louis, MO) in PBS plus 0.1% Trition X-100 for four hours at room temperature, followed by three 15 minutes washes of PBS plus Triton X-100. Dye exclusion experiments to test the integrity of the tracheal septate junctions were performed as described in Lamb et al., (1998). Confocal images were acquired on a Zeiss LSM510 Meta Laser Scanning Confocal Microscope (Carl Zeiss Inc, Thornwood, NY). Photomicrographs were adjusted for brightness and contrast with the Adobe Photoshop, and figures were compiled in Adobe Illustrator.

Results

uninflatable encodes a novel transmembrane protein that is highly conserved in insect species

We identified an EMS-induced mutation that failed to complement the molecularly defined deficiency *Df(2L)Exel7029* (cytology 27C4;27D4), and showed primarily larval lethality characterized by poorly inflated tracheae. Sequence analysis of genomic DNA isolated from mutant embryos revealed a nonsense mutation in the gene *CG9138* (also known as *SP1070*; CG to TA transition at nucleotide 29974 of GenBank sequence **AC008326** generating a Gln^{2407} to stop mutation; Fig. 1A). Based upon the defective tracheal inflation phenotype (described in more detail below), we renamed the gene *uninflatable* (*uif*). We recovered two additional alleles of *uif* through an F_2 screen of EMS-induced mutations. Sequence analysis indicated that uif^{1A15} results from a missense mutation changing Val^{1424} into Glu (TA to AT transversion at nucleotide 31022 of GenBank sequence **AC008326**), whereas uif^{2B7} results in a nonsense mutation (Gln^{1741}-stop; CG to TA transition at nucleotide 27955 of GenBank sequence **AC008326**; Fig. 1A).

The predicted Uif protein contains 3557 amino acids with a molecular mass of ~380 KD (Fig. 1A). Details of the genomic organization of *uif* can be found in the supplemental materials (Supplemental Fig. 1). Uif possesses a signal sequence at the amino terminus and contains a single transmembrane domain from amino acids 3415-3437 (based on TMHMM; Krogh et al., 2001), generating a Type I transmembrane protein. The large extracellular domain contains one C-type lectin-like (CLECT) domain (a domain known to function in carbohydrate binding), three CUB domains (a structural motif of unknown function often found in extracellular or plasma membrane proteins with developmental roles), three complement control protein (CCP) domains (likely protein

interaction domains found in a number of complement proteins and adhesion molecules), and one coagulation factor 5/8 C-terminal (FA58C) domain (another putative carbohydrate binding domain). In addition, the extracellular domain contains three hyaline repeat (HYR) domains (an immunoglobulin fold domain likely involved in cell adhesion), seven GCC2_GCC3 domains (cysteine-rich domains of unknown function), seven calcium binding EGF-like domains (protein interaction domains often involved in cell signaling), and one laminin-G domain (a domain found in a number of proteins involved in cell adhesion and signaling) (Fig. 1A). The transmembrane domain contains a GxxxG transmembrane helix dimerization domain (Russ and Engelman, 2000), suggesting that Uif might exist as a dimer or in higher order protein complexes at the membrane.

Uif is highly conserved in insect species, but does not appear to have a true ortholog in vertebrate species. Through BLAST searching we found a single Uif protein in each of the insect species shown in Fig. 1B. The domain organization and relative positions of the conserved extracellular domains are identical in all of these species. The Uif proteins found in *Drosophila melanogaster* and *Acyrthosiphon pisum* (Pea Aphid), which last shared a common ancestor ~350 million years ago (Consortium, 2006), are 69% identical with 82% similarity and only 1% gaps. The cytoplasmic domain, which is devoid of any conserved domains, share >80% sequence identity in all the insect species shown in Fig. 1B, but cannot be identified by homology searches outside of the insect class.

uif is required for embryonic tracheal inflation

Genetic evidence suggests that uif^{2B7} is an amorphic allele, consistent with the sequence analysis showing a premature stop codon in the extracellular domain. Specifically, uif^{2B7} shows an identical level of embryonic lethality to $uif^{2B7}/Df(2L)Exel7029$ (~15%), and all the animals that hatch in both genotypes die as larvae (Table 1). Cuticle preparations of the dead embryos in both genotypes

showed mostly normal cuticular structures. Specifically greater than 90% of *uif*^{2B7}*/Df(2L)Exel7029* dead embryos showed no obvious patterning defects nor defects in morphogenesis including germ band retraction, dorsal closure or head involution, with the remaining embryos showing mild defects in head involution (*n*=27 mutant embryos; data not shown). Similarly, 83% of *uif*^{2B7} dead embryos showed no obvious defects with the remaining 17% showing head involution or mild head skeleton defects (*n*=41 mutant embryos; data not shown). In contrast, *uif*^{1A15} is likely a hypomorphic allele since homozygous mutant animals show almost no embryonic lethality, but still display a nearly completely penetrant larval lethality, while *uif*^{1A15}*/Df(2L)Exel7029* mutant animals again show 13% embryonic lethality (Table 1).

One completely penetrant phenotype found in all unhatched embryos and newly hatched larvae for all of these mutations was a failure in tracheal inflation (Fig. 2B and data not shown). Although the penetrance of this phenotype is complete, the expressivity is variable, ranging from animals having completely uninflated trachea to animals having only a small section of uninflated trachea. The entire range of expressivity was found in both genotypes. Brightfield and differential interference contrast (DIC) microscopy of the mutant animals clearly showed that the tracheae were present. Notably, the junctions between inflated and non-inflated regions of the dorsal trunk did not correlate with the location of fusion between adjacent tracheal metameres. In addition, although in general the tube length and diameter appeared to be mostly normal, we did notice localized irregularities in the tracheae of mutant larvae, including twists, constrictions, and crumpled dorsal trunks (Figs. 2H-J).

As a means to demonstrate that the tracheal inflation defects resulted from loss of *uif*, we used the UAS-GAL4 system (Brand and Perrimon, 1993) to express a double stranded *uif* RNA construct either ubiquitously in the embryo (using *daughterless-Gal4*), specifically in the developing tracheal system (using *breathless-Gal4*) or in all the posterior segments of the embryo, but not in tracheae

(since the trachea invaginate from placodes in the anterior compartment of each segment; using *engrailed-Gal4*). Expression studies indicated that *btl>uifRNAi* strongly and specifically reduced Uif protein levels in tracheae (Supplemental Fig. 3). Using either the *da-* or *btl-Gal4* line to induce *uifRNAi*, we observed 5-20% embryonic lethality, with the majority of the hatched embryos dying as larvae (Table 1). Importantly, we also observed a nearly completely penetrant tracheal inflation defect in both cases (Figs. 2C-E). Similar to the *uif* loss of function alleles described above, the inflation defects showed variable expressivity with both *Gal4* lines used. For example some *btl>uifRNAi* animals showed mostly inflated tracheae (Fig. 2C), whereas other animals had completely uninflated tracheae (Fig. 2D). Neither *da-Gal4/+*, *btl-Gal4/+* nor *uif RNAi/+* animals showed any tracheal inflation defects. In contrast, *en>uifRNAi* animals showed no embryonic lethality and had completely inflated tracheae ($n > 50$ animals, Fig. 2F), even though the *uifRNAi* strongly reduced Uif expression in epithelial cells (data not shown). Therefore, the phenocopied tracheal inflation defects by *uifRNAi* specifically in the trachea, the lack of tracheal inflation defects associated with *uifRNAi* in posterior compartments of the epidermis, and with the genetic results showing completely penetrant tracheal inflation defects in *uif* homozygous, hemizygous and transheterozygous animals strongly argues that these defects result from specific loss of *uif* function in tracheal cells.

To determine whether the tracheal inflation defects in uif^{2B7} mutant animals resulted from a failure to establish an inflated tracheal system in late embryos or the ability to maintain fully inflated tracheae in early larval life, we used live imaging to monitor tracheal inflation in mutant embryos. As shown in Supplemental Movie 1 and Fig. 3, tracheal inflation begins in late stage 17 after the embryo begins to experience dramatic muscular contractions. In the uif^{2B7} embryo shown in Fig. 3, complete inflation of the dorsal trunk occurred over a 7-minute period, whereas there was little or no inflation of tracheal branches distal to the transverse connective in each segment. The

dynamics of tracheal inflation are in strong agreement with that found in wild type animals, which was shown to result in complete inflation of the tracheal system in ~10 minutes (Tsarouhas et al., 2007). There was no additional inflation of the *uif*^{2B7} tracheae over the next 173 minutes, after which the animal hatched and crawled away. In all, we imaged more than 30 *uif*^{2B7} mutant animals and observed either no inflation, or partial inflation that occurred over a short period of time (<10 minutes) and then remained unchanged throughout the period of observation (Supplemental Movie 1 and data not shown). We additionally collected newly hatched *uif*^{2B7} first instar larvae, separated them into individual apple juice plates, and recorded the degree of tracheal inflation two to three times per day for two days. We observed no obvious changes in the degree of tracheal inflation over those two days (data not shown). Thus we conclude that the tracheal inflation defects seen in *uif* mutant larvae result from a defect in the establishment of inflated tracheae during embryogenesis rather than a defect in maintaining inflated tracheae throughout embryogenesis or into larval life.

Tracheal morphogenesis and maturation are unaffected in uif mutant embryos

How might tracheal inflation defects arise in *uif* mutant embryos? It is possible that a defect in tracheal morphogenesis or tube maturation may lead to tubes that are open to the hemocoel or are physically obstructed, thereby preventing complete air filling. To address these possibilities we examined tracheal morphogenesis and maturation in *uif* mutant animals. Here we are presenting the results from our analysis of the amorphic allele *uif*^{2B7}, although identical results were observed with the hypomorphic allele *uif*^{1A15} (data not shown). Embryos stained with monoclonal antibody 2A12 that recognizes an epitope on the tracheal lumen revealed that tracheal patterning and tube size control are normal in *uif*^{2B7} mutant embryos (Fig. 4). Specifically, the metameric pattern of dorsal trunk, dorsal branch, lateral trunk and visceral branch are present and indistinguishable between

uif^{2B7} and *uif*^{2B7}/+ embryos (Figs. 4A, B and data not shown). Fusion of adjacent metameres was also observed by the correct formation of a three ring E-Cadherin structure at the junction of the two fusion cells (data not shown, but note the three ring structure of these cells by Crumbs staining in *uif*^{2B7} and *uif*^{1A15} mutant embryos in Supplemental Fig. 3). By stage 16, the diameter of the dorsal trunk in *uif*^{2B7} mutant embryos had expanded to the same degree as it had in *uif*^{2B7}/+ embryos, and the length of the dorsal trunk was similar between *uif*^{2B7} and *uif*^{2B7}/+ embryos (Figs. 4A, B). Since tube diameter expansion and tube length regulation both require the secretion of chitin into the lumen of the trachea, followed by subsequent endocytosis of the chitin, we stained *uif*^{2B7} mutant embryos with chitin binding probe (CBP), wheat germ agglutinin (WGA) and Congo Red to verify that these events occurred normally in *uif* mutant embryos. CBP staining demonstrates that the chitin is secreted into the lumen of *uif*^{2B7} mutant tracheal tubes and forms a continuous dense cable through the trachea at stage 16 (Figs. 4C, D). Note also that the cable is continuous through the fusion cells joining adjacent metameres, further demonstrating that fusion and cavitation of the dorsal tube had occurred. By stage 17, chitin had been cleared from the center of the tracheal lumen and CBP only recognizes the apical surfaces of the tracheae, exactly as observed in *uif*^{2B7}/+ animals (Figs. 4E, F). We similarly observed a thick chitin cable in stage 16 *uif*^{2B7} mutant embryos using WGA and Congo Red, with only residual staining on the apical surface of stage 17 embryos (data not shown), suggesting that endocytosis of tracheal luminal material had occurred normally in *uif* mutant embryos.

Another possible mechanism that could result in liquid permeable trachea is a defect in the paracellular barrier function of the septate junction in tracheal cells. Intact septate junctions are necessary for the secretion of chitin modifying enzymes into the tracheal lumen and thus play critical roles in tube diameter and length control (described in introduction). However, Paul et al., (2003) demonstrated that there is not a perfect correlation between the septate junction barrier

function and tube size control, and thus although tube size control appears normal in *uif* mutants, it is possible that Uif could specifically affect the barrier function of the septate junction. To address this possibility we stained uif^{2B7}/+ and uif^{2B7} mutant embryos with antibodies against the septate junction proteins Coracle (Cor), Fasciclin III, and Discs Large to assess the integrity of this junction. All three septate junction proteins were correctly localized in the trachea, salivary glands and epidermis of uif^{2B7} mutant embryos (Figs. 4G-J and data not shown). To test the paracellular barrier function of the septate junctions we performed a dye permeability assay (Lamb et al., 1998). We found that a 10 kD Rhodamine-labeled dextran injected into the hemocoel of stage 16 uif^{2B7} mutant embryos failed to cross the salivary gland and tracheal epithelium into the lumen, indicating that the septate junctions were functionally tight in these animals (data not shown). Taken together, these results demonstrate that tracheal morphogenesis and tube maturation occur normally in *uif* mutant embryos, and that the tracheal inflation defects are likely not a consequence of impaired development of the trachea during embryogenesis.

uif is required for larval tracheal growth and tracheal molting

All uif^{2B7} and most uif^{1A15} mutant animals that hatch as larvae die prior to pupariation, with the majority dying as small first instar larvae. We examined three independent cohorts of uif^{2B7} (n=226 mutant animals) and uif^{1A15} (n=124) mutant animals five days after hatching and determined that 25% ($\pm$ 6%) of the uif^{2B7} and 40% ($\pm$ 7%) of the uif^{1A15} were still alive. Interestingly, only 13% ($\pm$ 6%) of the uif^{2B7} and 27% ($\pm$ 10%) of the uif^{1A15} mutants had advanced to third instar. It was not uncommon to find mutant third instar larvae that were more than 10 days post hatching. The mutant larvae did grow much slower than their heterozygous siblings and typically the largest mutant larvae were only about half the size of their siblings at the time when their siblings pupariated (Fig.

5A). A larger percentage of *uif*^{1A15} larvae grow to this larger size than *uif*^{2B7} mutant larvae, consistent with the suggestion that *uif*^{2B7} is an amorphic allele, whereas *uif*^{1A15} is a strong hypomorphic allele. Interestingly, *btl>uifRNAi* larvae also displayed this strong growth defect, whereas *btl-GAL4/+* and *UAS-uifRNAi/+* larvae did not (data not shown). It is possible that this larval growth defect is associated with hypoxia as we observed that mutant larvae (*uif*^{2B7}, *uif*^{1A15}, and *btl>uifRNAi*) spend very little time in the food and instead wander around the plate, even if they appear to have mostly inflated trachea. Wingrove and O'Farrell (1999) noted similar behavioral responses to hypoxia in larvae. One consequence of this wandering away from food behavior is that the mutant larvae accumulate much less fat and are more transparent than their heterozygous siblings (Figs. 5B and C).

An examination of *uif* mutant third instar larvae (*uif*^{2B7}, *uif*^{1A15}, and *btl>uifRNAi*) revealed a strong reduction in tracheal tube length (Figs. 5B, C and data not shown). Whereas *uif* mutant tracheal tube length and diameter were indistinguishable from wild type prior to inflation (Figs. 4A, B) and still were of wild type size in newly hatched larvae (Figs. 2A, B), third instar *uif* tracheae were substantially shorter than those in wild type larvae (even of second instar of comparable size; Figs. 5B, C). The most obvious manifestation of this defect was the location of the transverse connective (TC) relative to the body segments. In wild type second and third instar, each abdominal segment had one TC emanating from each dorsal trunk (Fig. 5B). In contrast, in *uif* mutant third instar larvae, most of the TCs emanated from portions of the dorsal trunk that corresponded to the final two abdominal segments, with the visceral branches and lateral trunk stretching far anteriorly to tracheate the correct segment (Fig. 5C). To gain a quantitative measure of the severity of this growth defect we compared partial tracheal length (along the dorsal trunk from the posterior spiracle to the TC that originated in abdominal segment 4 during embryogenesis) to full body length for w^{1118} and *uif* mutant larvae (Table 2). Interestingly, this ratio did not change in w^{1118} from

second to third instar larvae and thus does not appear to be influenced by developmental stage. We found that *uif* mutant third instar larvae had substantially reduced relative tracheal length, at least in the posterior half of the trachea, compared to wild type larvae (Table 2).

Microscopy of live uif^{2B7} mutant second instar larvae revealed a tracheal molting defect in which two tracheal cuticle layers were clearly present with only the first instar trachea being inflated (Fig. 5D). To more closely examine this tracheal molting defect we dissected portions of the dorsal trunk from w^{1118} and uif^{2B7} and uif^{1A15} third instar larvae and examined them by DIC microscopy. Notably, the *uif* mutant tracheae were substantially more brittle than w^{1118} trachea. Both *uif* mutations showed a completely penetrant defect in tracheal molting in which at least two distinct tracheal cuticles were present and occasionally three cuticular layers could be observed. The tracheal molting defect was always detected in the posterior segments closest to the spiracles, but was not always observed in more anterior segments (data not shown). We also observed a weakly penetrant epidermal molting defect in which the previous cuticle remained affixed to the larva at its posterior spiracles (Fig. 5E), possibly related to this tracheal molting defect. We inspected the organization of the taenidia in these dissected tracheae by DIC microscopy and found that the tightly packed parallel rows of taenidia were present in the tracheae of uif^{1A15} and uif^{2B7} mutant larvae, although the density of the taenidia appeared lower in uif^{2B7} mutant larvae and there were some local irregularities, most notably regions where the rows converged and appeared to cross each other (Fig. 5G). In addition, the taenidia remain in focus for a greater depth in the Z-axis of wild type dorsal trunks than in uif^{2B7} mutant larvae, suggesting that the taenidia might be shallower in mutant tracheae compared to wild type (Figs. 5F, G).

Uif localizes to the apical plasma membrane in ectodermally derived epithelia

We performed both RNA *in situ* hybridization and immunostaining of w^{1118} embryos to determine the tissue distribution of *uif* RNA and Uif protein, as well as the subcellular localization of the protein. Expression of *uif* RNA is first detected in stage 5 embryos in cells that are fated to become ectodermal (Supplemental Fig. 2). *uif* is noticeably reduced or absent in mesodermal and neurectodermal precursors. In later stage embryos, *uif* expression persists in ectodermal tissues and is very strongly expressed in the developing tracheal system. We generated a polyclonal antiserum against a unique region of the extracellular domain (noted on Fig. 1). This antiserum appears specific as it recognizes an epitope in w^{1118} embryos (Fig. 6), but not in uif^{2B7} or *Df(2L)Exel7029* mutant embryos (Supplemental Fig. 3 and data not shown). Interestingly, the antiserum recognizes a protein that is strongly expressed in the tracheae in uif^{1A15} mutant embryos, but rather than localizing to the plasma membrane, the protein remains inside the cell (Supplemental Fig. 3). In wild type embryos, Uif is first detected in the cephalic furrow and ventral furrow at stage 7 (data not shown). Subsequently, Uif staining is detected in the epidermis, foregut, hindgut, salivary gland and is particularly robust in the trachea (Fig. 6). We stained wild type larvae and found that Uif expression persists at high levels in the tracheal system, and is also abundant in the foregut and hindgut (data not shown). In larvae, Uif expression is also present at high levels in the imaginal discs and at lower levels in the epidermis, but is not obviously expressed in the salivary glands. In the adult, we found no expression of Uif in oocytes or in follicle cells (data not shown). The lack of *uif* RNA and Uif protein in early embryos, coupled with the lack of Uif expression in oocytes suggests that *uif* expression is from zygotic transcription and that there is no maternal contribution.

Subcellularly, Uif localizes to the apical plasma membrane. To determine if Uif spreads into the lateral junctions, we costained w^{1118} embryos with antibodies that recognize Uif and markers for the adherens junction (Armadillo, Arm), septate junction (Coracle, Cor) and the marginal zone (Crumbs, Crb). Uif was found to be more apically localized than Arm and Cor in every embryonic

tissue that it was expressed (data not shown). Uif partially co-localizes with Crb in the marginal zone of embryonic epidermal cells, but as detected in cross section views, is also strongly expressed on the apical plasma membrane in a domain where Crb expression is lower (Fig. 6B). This apical plasma membrane localization of Uif is most apparent in the tracheal system where Uif localizes in a domain more apical than Crb. For example, during stage 11 when the tracheal placode is invaginating, Uif is clearly on the apical plasma membrane in a domain distinct from that labeled by Crb (Fig. 6C). Similarly, in the dorsal tracheal trunk of stage 14 embryos, Uif protein appears to define the apical lumen of the trachea, whereas Crb staining maintains a cross hatched appearance that defines the marginal zone of the tracheal cells (Fig. 6D).

Discussion

In this report we have described the initial characterization of a novel gene, *uninflatable*, which encodes a single-pass type I transmembrane protein with several different carbohydrate binding motifs and epidermal growth factor repeats in its extracellular domain. This gene is highly conserved in insect species, but does not appear to have a true ortholog in mammals or other vertebrate organisms. Uninflatable is expressed on the apical surface of ectodermally-derived epithelial cells including the epidermis, trachea, salivary gland and fore- and hindgut, although it is most highly expressed in tracheal epithelia starting as the tracheal placode invaginates and persisting throughout its development. We isolated three mutant alleles of *uif*, and found that the predominant defects associated with loss of *uif* were defective air inflation at the end of embryogenesis, and tracheal growth and tracheal molting defects in larvae.

Functions of uif during embryogenesis

The most obvious defects observed in *uif* mutant late embryos and newly hatched first instar larvae were incomplete inflation of the trachea coupled with tracheal tubes that often appeared pinched or stretched (Fig. 2). Live imaging of individual *uif* mutant embryos and larvae revealed that these tracheal inflation defects result from the inability to completely inflate the trachea at the end of embryogenesis rather than a defect in the maintenance of an inflated tracheal system after hatching (Fig. 3 and supplemental movie 1). Interestingly, tracheae in *uif* mutant embryos are normally patterned and appear to mature in a manner indistinguishable to tracheae in wild type animals (Fig. 4). Thus this tracheal inflation defect likely results from a requirement for *uif* function late during embryogenesis.

Several genes have been characterized whose defects include incomplete tracheal inflation. Included in these genes are those that function at the end of embryogenesis to clear the trachea of solid luminal material. This process requires clathrin-mediated endocytosis and includes the proteins clathrin heavy chain, the GTPase dynamin (encoded by *shibire*), and a clathrin binding transmembrane protein encoded by *wurst* (Behr et al., 2007). Notably, mutations in all of these genes also result in elongated tracheal tubes suggesting a defect in tracheal tube size control. Gas filling defects were also observed by Behr et al., (2007) for mutations in *serp* and *verm*, two putative matrix chitin deacytlases that function to regulate tracheal tube length (Luschnig et al., 2006; Wang et al., 2006). Tracheal maturation appears normal in *uif* mutant embryos, including the secretion of chitin into the tracheal lumen and the subsequent uptake of luminal solids near the end of embryogenesis (as indicated by chitin binding probe staining in Fig. 4, and WGA and Congo Red staining that were not shown). In addition, *uif* mutant tracheae do not show diameter or length defects during embryogenesis, suggesting that the luminal chitin cylinder forms normally and that Serp and Verm are correctly functioning during the maturation process. Taken together these results suggest that the air filling defects observed in *uif* mutant embryos occurs through a mechanism independent of that linked to endocytosis of solid luminal material.

A second class of proteins that likely function in proper air inflation is the epithelial sodium channels (ENaCs). In mammals, ENaC proteins are required to help remove liquid from embryonic lung prior to birth (Hummler et al., 1996). There are 16 *ENaC* genes (also referred to as *pickpocket* or *ppk* genes) in the *Drosophila* genome, of which 9 are expressed in the embryonic tracheal system (Liu et al., 2003). It is thought that the influx of sodium through these channels drives water from the lumen into the epithelial cells, and that degassing of this liquid inflates the trachea. Although there are no loss of function mutations in ENaCs that result in air filling defects in *Drosophila*, RNA interference mediated knockdown of *ppk4* and *ppk11* results in partially liquid-filled tracheae

in larvae (Liu et al., 2003). In addition, inhibiting these channels using amiloride also results in fluid filled tracheae in larvae. Although both of these examples affected air filling after a molt, it seems likely that ENaC proteins may also contribute to air filling at the end of embryogenesis. At this point we cannot exclude the possibility that *uif* may regulate the expression or activity of *ENaC* encoded proteins in tracheal epithelia.

A third possibility, and one that we favor, is that *uif* is playing primarily a structural role in embryonic tracheal maturation. Two pieces of evidence support this notion. First, in early stage 17 mutant embryos the tracheae are of normal length and diameter and have a stereotypic appearance that is indistinguishable from that of wild type animals, whereas in newly hatched mutant larvae the tubes are often crushed or twisted (Fig. 2). Second, while dissecting tracheae from wild type and *uif* mutant third instar larvae it was clear that the mutant tracheae were more brittle. Wild type tracheae have an elastic property that makes them difficult to break, whereas we had to be very careful dissecting *uif* tracheae in order to get a section that included more than one metameric unit. Together these observations suggested a model in which the mechanical properties of *uif* mutant tracheae are compromised, thereby allowing the tracheal cuticle to fail when the embryo initiates violent muscular contractions prior to hatching. As noted in the live imaging, tracheal inflation initiates well after the embryo begins these dramatic muscular contractions. We predict that a combination of crushed tubes and small cracks in the tracheal cuticle prevent complete inflation.

Functions of uif in larvae

uif mutant larvae that survive to second or third instar show striking defects in tracheal growth and tracheal molting. The tracheae in these *uif* mutant larvae have short dorsal trunks that are well out of proportion to the body length of the animal (Fig. 5 and Table 2). It is difficult to accurately assess

the diameter of the dorsal trunk in these animals, however, because the mutant animals fail to completely shed their tracheal cuticle, and often only the first instar lumen is inflated. This tracheal molting defect was nearly completely penetrant in all third instar *uif*^{2B7} and *uif*^{1A15} mutant larvae examined, but the severity seemed to vary along the anterior-posterior axis, with some middle and anterior sections showing no molting defects, whereas the sections near the posterior spiracles showed at least two and sometimes three tracheal cuticles. Beitel and Krasnow (2000) conducted morphometric analyses of larval tracheal growth and observed that tracheae lengthen in a continuous fashion, whereas the diameter increases in a stepwise manner coincident with the molt, suggesting that tube length is controlled independently from tube diameter. Our results indicate that *uif* plays a role in regulating the growth of the tracheae along their length.

How might *uif* regulate larval tracheal tube length? One possibility is that Uif might regulate the interface between the tracheal epithelium and the cuticle, possibly by providing lubrication through its hyalin domains. Loss of *uif* would therefore result in a situation where the epidermis is too tightly bound to the overlying cuticle to allow for growth along the long axis of the tracheae. This type of mechanism could also account for the tracheal molting defects and thereby couple these phenotypes. Page-McCaw et al., (2003) identified mutations in the Matrix Metalloproteinase encoded by *Mmp1* and found similar defects in tracheal elongation. They also speculated that the *Mmp1* tracheal defects might be caused by the inability of the tracheal epithelial cells to loosen their attachment to the cuticle. Since *uif*^{2B7} mutant larvae have no full length Uif protein, it is unlikely that Uif is a primary target of MMP1 in tracheal cells. In addition, we observed no genetic interaction between *uif* and *Mmp1* by second-site noncomplementation (data not shown).

An alternative hypothesis is that Uif might serve as a receptor or co-receptor for a systemic signal that couples tracheal growth with larval growth. The extracellular domain of Uif contains multiple EGF domains and a laminin G domain, and the cytoplasmic domain is remarkably

conserved in all insect species. A combination of structure/function analysis and genetic and biochemical approaches to identify Uif interacting proteins should help to shed light on this functions of *uif*. Understanding how Uif couples tracheal growth to the growth of the larva may serve as an important paradigm for similar couplings of organ growth to organismal growth in other species.

Finally, hypoxia may account for all the other larval phenotypes associated with loss of *uif*, including early larval lethality, slow growth, developmental arrest and failure to pupariate. Most *uif* mutant larvae die as first instars, and those that die early almost invariably have the most severe tracheal inflation defects. *uif* mutant larvae that survive to second or third instar grow much slower than their heterozygous siblings (Fig. 5A). *btl>uifRNAi* larvae that have only lost *uif* function in their tracheae show an identical slow growth phenotype. We consistently observed *uif* mutant larvae wandering away from food, suggesting that they were experiencing hypoxia (Wingrove and O'Farrell, 1999). Not surprisingly these larvae accumulate less fat and have a transparent appearance (Fig. 5C). Examination of the tracheae in these mutant animals revealed that the inflated portion of the trachea was often just through the first instar tracheal lumen (Fig. 5D), and therefore these animals were likely oxygen starved as well. Consistent with this notion, we observed additional tracheal branching in these mutant animals suggesting that the hypoxia induced factor pathway had been engaged (data not shown). Thus, hypoxia could explain the growth defects observed in *uif* mutant larvae. These growth defects may have then resulted in the observed developmental delays. For example, mutant third instar larvae may not have reached a critical weight threshold needed for pupariation, and thus would not have been able to pupariate even if they experienced the metamorphic pulse of ecdysone (we have not determined if they received this signal). Interestingly, many *uif* mutant animals even failed to advance to third instar, but this did not reflect a defect in epidermal molting or ecdysis, as we found no evidence for an extra set of head

skeleton or epidermal cuticle. Rather the animals just arrested as first or second instars. It is possible that hypoxia-induced growth defects contributed to this phenotype as well, since larvae have to attain a critical size to be competent for molting, just as they do for pupariation (Nijhout, 1981).

Acknowledgments

We thank Ty Beaver for help with the F_2 screen for new *uif* alleles, Aaron Welch for help with the mapping of *uif*, Paulyn Cartwright for help with the phylogenetic analysis and photography of *in situ* hybridized embryos, and Kirsten Jensen for help with the permanent mounting of 2A12 stained specimens. We are grateful to Greg Bietel, the Bloomington *Drosophila* Stock Center and the Vienna *Drosophila* RNAi Center for fly stocks used in this study. We thank Richard Fehon and the Developmental Studies Hybridoma Bank for the antibodies used in this study. We thank Greg Bietel, Brian Ackley, Erik Lundquist, Robert Cohen and John Ewer for insightful discussions about the study, an anonymous reviewers for suggestions that improved the manuscript. The project was supported by NIH Grant Number P20 RR15563 and NIH Grant Number R01HD047570 from the National Center for Research Resources.

References

Affolter, M., and Caussinus, E. (2008). Tracheal branching morphogenesis in Drosophila: new insights into cell behaviour and organ architecture. *Development* **135,** 2055-2064.

Araujo, S. J., Aslam, H., Tear, G., and Casanova, J. (2005). mummy/cystic encodes an enzyme required for chitin and glycan synthesis, involved in trachea, embryonic cuticle and CNS development--analysis of its role in Drosophila tracheal morphogenesis. *Dev. Biol.* **288,** 179-193.

Behr, M., Riedel, D., and Schuh, R. (2003). The claudin-like megatrachea is essential in septate junctions for the epithelial barrier function in Drosophila. *Dev. Cell* **5,** 611-620.

Behr, M., Wingen, C., Wolf, C., Schuh, R., and Hoch, M. (2007). Wurst is essential for airway clearance and respiratory-tube size control. *Nat. Cell Biol.* **9,** 847-853.

Beitel, G. J., and Krasnow, M. A. (2000). Genetic control of epithelial tube size in the Drosophila tracheal system. *Development* **127,** 3271-3282.

Brand, A. H., and Perrimon, N. (1993). Targeted gene expression as a means of altering cell fates and generating dominant phenotypes. *Development* **118,** 401-415.

Choksi, S. P., Southall, T. D., Bossing, T., Edoff, K., de Wit, E., Fischer, B. E., van Steensel, B., Micklem, G., and Brand, A. H. (2006). Prospero acts as a binary switch between self-renewal and differentiation in Drosophila neural stem cells. *Dev Cell* **11,** 775-89.

Consortium, T. H. G. S. (2006). Insights into social insects from the genome of the honeybee Apis mellifera. *Nature* **443,** 931-949.

Devine, W. P., Lubarsky, B., Shaw, K., Luschnig, S., Messina, L., and Krasnow, M. A. (2005). Requirement for chitin biosynthesis in epithelial tube morphogenesis. *Proc. Natl. Acad. Sci. U S A* **102,** 17014-17019.

Dietzl, G., Chen, D., Schnorrer, F., Su, K. C., Barinova, Y., Fellner, M., Gasser, B., Kinsey, K., Oppel, S., Scheiblauer, S., Couto, A., Marra, V., Keleman, K., and Dickson, B. J. (2007). A genome-wide transgenic RNAi library for conditional gene inactivation in Drosophila. *Nature* **448,** 151-156.

Edgar, R. C. (2004). MUSCLE: multiple sequence alignment with high accuracy and high throughput. *Nucleic Acids Res.* **32,** 1792-1797.

Fehon, R. G., Dawson, I. A., and Artavanis-Tsakonas, S. (1994). A Drosophila homologue of membrane-skeleton protein 4.1 is associated with septate junctions and is encoded by the coracle gene. *Development* **120,** 545-557.

Fehon, R. G., Johansen, K., Rebay, I., and Artavanis-Tsakonas, S. (1991). Complex cellular and subcellular regulation of notch expression during embryonic and imaginal development of *Drosophila*: implications for notch function. *J Cell Biol* **113,** 657-669.

Hummler, E., Barker, P., Gatzy, J., Beermann, F., Verdumo, C., Schmidt, A., Boucher, R., and Rossier, B. C. (1996). Early death due to defective neonatal lung liquid clearance in alpha-ENaC-deficient mice. *Nat. Genet.* **12,** 325-328.

Kerecuk, L., Schreuder, M. F., and Woolf, A. S. (2008). Renal tract malformations: perspectives for nephrologists. *Nat. Clin. Pract. Nephrol.* **4,** 312-325.

Krogh, A., Larsson, B., von Heijne, G., and Sonnhammer, E. L. (2001). Predicting transmembrane protein topology with a hidden Markov model: application to complete genomes. *J. Mol. Biol.* **305,** 567-580.

Lamb, R. S., Ward, R. E., Schweizer, L., and Fehon, R. G. (1998). Drosophila coracle, a member of the protein 4.1 superfamily, has essential structural functions in the septate junctions and developmental functions in embryonic and adult epithelial cells. *Mol. Biol. Cell* **9,** 3505-3519.

Le, T., Liang, Z., Patel, H., Yu, M. H., Sivasubramaniam, G., Slovitt, M., Tanentzapf, G., Mohanty, N., Paul, S. M., Wu, V. M., and Beitel, G. J. (2006). A new family of Drosophila balancer chromosomes with a w- dfd-GMR yellow fluorescent protein marker. *Genetics* **174,** 2255-2257.

Liu, L., Johnson, W. A., and Welsh, M. J. (2003). Drosophila DEG/ENaC pickpocket genes are expressed in the tracheal system, where they may be involved in liquid clearance. *Proc. Natl. Acad. Sci. U S A* **100,** 2128-2133.

Llimargas, M., Strigini, M., Katidou, M., Karagogeos, D., and Casanova, J. (2004). Lachesin is a component of a septate junction-based mechanism that controls tube size and epithelial integrity in the Drosophila tracheal system. *Development* **131,** 181-190.

Luschnig, S., Batz, T., Armbruster, K., and Krasnow, M. A. (2006). serpentine and vermiform encode matrix proteins with chitin binding and deacetylation domains that limit tracheal tube length in Drosophila. *Curr. Biol.* **16,** 186-194.

Matusek, T., Djiane, A., Jankovics, F., Brunner, D., Mlodzik, M., and Mihaly, J. (2006). The Drosophila formin DAAM regulates the tracheal cuticle pattern through organizing the actin cytoskeleton. *Development* **133,** 957-966.

Nijhout, H. F. (1981). Physiological control of molting in insects. *Am. Zool.* **21,** 631-640.

Page-McCaw, A., Serano, J., Sante, J. M., and Rubin, G. M. (2003). Drosophila matrix metalloproteinases are required for tissue remodeling, but not embryonic development. *Dev. Cell* **4,** 95-106.

Paul, S. M., Ternet, M., Salvaterra, P. M., and Beitel, G. J. (2003). The Na+/K+ ATPase is required for septate junction function and epithelial tube-size control in the Drosophila tracheal system. *Development* **130,** 4963-4974.

Rasband, W. S. (1997-2009). ImageJ. *National Institutes of Health, Bethesda, MD, USA*.

Russ, W. P., and Engelman, D. M. (2000). The GxxxG motif: a framework for transmembrane helix-helix association. *J. Mol. Biol.* **296,** 911-919.

Shi, W., Bellusci, S., and Warburton, D. (2007). Lung development and adult lung diseases. *Chest* **132,** 651-656.

Tonning, A., Hemphala, J., Tang, E., Nannmark, U., Samakovlis, C., and Uv, A. (2005). A transient luminal chitinous matrix is required to model epithelial tube diameter in the Drosophila trachea. *Dev. Cell* **9,** 423-430.

Tsarouhas, V., Senti, K. A., Jayaram, S. A., Tiklova, K., Hemphala, J., Adler, J., and Samakovlis, C. (2007). Sequential pulses of apical epithelial secretion and endocytosis drive airway maturation in Drosophila. *Dev. Cell* **13,** 214-225.

Wang, S., Jayaram, S. A., Hemphala, J., Senti, K. A., Tsarouhas, V., Jin, H., and Samakovlis, C. (2006). Septate-junction-dependent luminal deposition of chitin deacetylases restricts tube elongation in the Drosophila trachea. *Curr. Biol.* **16,** 180-185.

Ward, R. E., Evans, J., and Thummel, C. S. (2003). Genetic modifier screens in Drosophila demonstrate a role for Rho1 signaling in ecdysone-triggered imaginal disc morphogenesis. *Genetics* **165,** 1397-1415.

Wingrove, J. A., and O'Farrell, P. H. (1999). Nitric oxide contributes to behavioral, cellular, and developmental responses to low oxygen in Drosophila. *Cell* **98,** 105-114.

Wu, V. M., and Beitel, G. J. (2004). A junctional problem of apical proportions: epithelial tube-size control by septate junctions in the Drosophila tracheal system. *Curr. Opin. Cell Biol.* **16,** 493-499.

Wu, V. M., Yu, M. H., Paik, R., Banerjee, S., Liang, Z., Paul, S. M., Bhat, M. A., and Beitel, G. J. (2007). Drosophila Varicose, a member of a new subgroup of basolateral MAGUKs, is required for septate junctions and tracheal morphogenesis. *Development* **134,** 999-1009.

Table 1
Lethal-phase analysis of *uif* mutant animals

Genotype	% Embryonic lethality[a] (*n*)[b]	% Larval lethality[a] (*n*)[b]
uif^{2B7}/*uif*^{2B7}	16 ± 1 (218)	100 (183)
uif^{1A15}/*uif*^{1A15}	3 ± 1 (180)	92 ± 3 (175)
uif^{1A15}/*uif*^{2B7}	10 ± 2 (228)	100 (204)
uif^{2B7}/*Df(2L)Exel7029*	15 ± 5 (140)	100 (177)
uif^{1A15}/*Df(2L)Exel7029*	13 ± 5 (140)	100 (122)
btl-Gal4/UAS-uifRNAi	5 ± 2 (260)	87 ± 6 (247)
UAS-uifRNAi/+; da-Gal4/+	18 ± 5 (294)	86 ± 2 (240)

[a] mean ± sd from three independent experiments
[b] total number of animals of indicated genotype that were scored

Table 2
Relative tracheal length in wild type and *uif* mutant larvae

Genotype	Partial tracheal length[a] / total body length (*n*)[b]
w^{1118}, 2nd instar	0.37 ± 0.02 (32)
w^{1118}, 3rd instar	0.37 ± 0.02 (26)
uif^{1A15}, 3rd instar	0.19 ± 0.03 (25)
btl-Gal4/UAS-uifRNAi, 3rd instar	0.24 ± 0.03 (14)

[a] Partial tracheal length = Distance along the dorsal trunk from the posterior spiracle to the TC that originated in body segment A4
[b] total number of animals of indicated genotype that were scored

Figure Legends

Fig. 1. Molecular organization and conservation of the *uninflatable* gene. (A) Predicted domain organization of Uif protein. A signal sequence is predicted at the N terminus and a single transmembrane (TM) domain is predicted near the C terminus. Molecular details of the mutant alleles are indicated. uif^{1} and uif^{2B7} result from premature stop codons, whereas uif^{1A15} results from a missense mutation changing Val^{1424} into Glu. CLECT, C-type lectin-like domain; CUB, complement C1r/C1s, Uegf, Bmp1 domain; CCP, complement control protein domain; FA58C, coagulation factor 5/8 C-terminal domain; HYR, hyaline repeat domain; EGF-CA, calcium binding Epidermal Growth Factor-like domain; Lam-G, laminin G domain. The region of Uif used for antibody generation is indicated by the bracket above the model. (B) Phylogenetic tree of Uif orthologs based upon full-length protein sequences. The sequence divergence of Uif correlates precisely with the evolutionary relationships found within the insect order, and no Uif homologs could be identified outside this order.

Fig. 2. *uif* mutant first instar larvae have defects in tracheal inflation and damaged tracheal tubes. (A-D) Brightfield photomicrographs of (A)w^{1118}, (B) uif^{2B7}, (C, D) *btl-Gal4/UAS-uifRNAi*, (E) *UAS-uifRNAi/+; da-Gal4/+*, (F) *en-Gal4/UAS-uifRNAi* newly hatched first instar larvae. All animals are depicted with anterior to the left. Refracted light makes the inflated trachea clearly visible in the wild type larva and shows that the tracheae of *uif* mutant animals are partially to completely uninflated. The boundary of inflated/uninflated trachea are marked by arrows in B, C and E. Note that *en>uifRNAi* larvae have normally inflated tracheae (F). (G-J) Differential Interference Contrast micrographs of dorsal tracheal trunks in w^{1118} (G) and uif^{2B7} (H-J) newly hatched first instar larvae. Note the regular diameter of the inflated dorsal trunk in the wild type larva as it gradually tapers towards the anterior over 6 segments, and contrast that to *uif* mutant

tracheae that appear twisted or crushed and show discontinuous regions that are uninflated. Scale bars = 50μm.

Fig. 3. *uif*^{2B7} mutant animals fail to establish fully inflated tracheae during embryogenesis. Selected brightfield photomicrographs from a time-lapse series of an *uif*^{2B7} mutant embryo showing a rapid period of tracheal inflation (A-E), followed by more than two hours with no additional inflation (F-I). Times given are relative to the start of observation which occurred in mid stage 17 of embryogenesis. The full time series can be seen in Supplemental movie1. Note that the inflation phase lasts for seven minutes and results in fully inflated dorsal trunks with little inflation distal to the transverse connectives in each metamere. Arrows indicate the extent of inflation of the dorsal trunk during the initial inflation phase. Arrowheads in D and H indicate the extent of inflation in three adjacent metameres and show that there is no additional inflation of these segments over a 166 minute period. Even though the animal has not completed tracheal inflation, it hatches and crawls away (J).

Fig. 4. *uif* mutant embryos have normal tracheal patterning and maturation, and have intact septate junctions. (A, B) 2A12 staining of stage16 *uif*^{2B7}/+ and *uif*^{2B7} embryos demonstrates that tracheal patterning as well as dorsal trunk tube length and diameter are normal in *uif* mutants at this stage of development. (C-F) Confocal optical sections of *uif*^{2B7}/+ and *uif*^{2B7} embryos stained with chitin binding probe (CBP) show a continuous chitin cable in the lumens of wild type and *uif* mutant animals at stage 16 (insets in C and D show xz projections of the dorsal trucks) that is completely cleared by mid-stage 17 (insets in E and F show optical cross sections of the dorsal trunk that can be visualized near the posterior of the animals). Note that CBP staining still outlines

the apical surface of the dorsal trunk in mid-stage 17 mutant embryos indicating the presence of a chitinous cuticle. (G-J) *uif*^{2B7}/+ and *uif*^{2B7} embryos stained with antibodies against the septate junction protein Coracle (Cor) show the correct localization of this protein in an *uif* mutant trachea (H) and salivary gland (J). In all panels, anterior is to the left. Scale bars = 50μm in A-B; 10μm in C-J.

Fig. 5. *uif* mutant second and third instar larvae have tracheal growth and molting defects. (A) Brightfield photomicrograph of a 5-day-old *w*^{1118} 3rd instar larva and a 5-day-old *uif*^{2B7} 3rd instar larva. Note the smaller overall size of the *uif*^{2B7} mutant larva. (B, C) Brightfield photomicrograph of a *w*^{1118} 2nd instar larva and a similarly sized *uif*^{2B7}*/Df(2L)Exel7029* 3rd instar larva showing a tracheal growth defect in the *uif* mutant larva. Red lines indicate the relative boundaries of the body segments, whereas red arrows indicate the junction of the transverse connective (TC) branch along the dorsal trunk in each metamere. Note that in the wild type larva one TC emanates from each dorsal trunk in each body segment, whereas in the *uif* mutant larva five TCs emanate from the dorsal trunk in the final two body segments. Also note that the *uif* mutant larva has less fat than the *w*^{1118} larva. (D) *uif* mutant larvae frequently fail to molt their tracheal cuticle. In this 5-day-old *uif*^{2B7} mutant 2nd instar larva the dashed lines indicate the basal membrane of the tracheal cells, whereas the dotted lines indicate the apical surface of the tracheal cells. Note the presence of two layers of cuticle with only the inner or 1st instar lumen being inflated. (E) *uif*^{2B7}*/Df(2L)Exel7029* mutant 3rd instar larva that has failed to complete its molt. The previous epidermal cuticle (arrow) is connected at the posterior spiracles. (F, G) DIC photomicrographs of *w*^{1118} and *uif*^{2B7} 3rd instar larval posterior dorsal tracheal trunks. Note the regular pattern of the taenidial folds in the wild type trachea. Although the trachea in G is uninflated, taenidia are present and are organized into roughly parallel

rows that run perpendicular to the long axis of the trachea. Scale bars = 100μm in B, C and E; 50μm in D, F and G.

Fig. 6. Uif is expressed on the apical plasma membrane of ectodermally derived epithelial cells during embryogenesis. (A) Open pinhole confocal micrograph of a stage 15 w^{1118} embryo double labeled with anti-Uif (green) and anti-Crb (red) antibodies. Individual channels are shown for Uif (A') and Crb (A''). Uif expression can be detected in the fore- and hindgut, the epidermis and most strongly in the tracheal system. (B-D) Higher magnification confocal optical sections of w^{1118} embryos stained with anti-Uif (green) and anti-Crb (red) antibodies. Individual channels are shown for Uif (') and Crb ('). Tissues include the epidermis at stage 14 (B-B"), the tracheal placode at stage 11 (C-C"), and the tracheal dorsal trunk at stage 14 (D-D"). Note that Uif is expressed in a domain that is more apical than Crbs in all of these tissues. In all cases anterior is to the left. In panel B apical is up. In panel C apical is to the center of the placode. Scale bars = 50μm in A; 10μm in B-D.

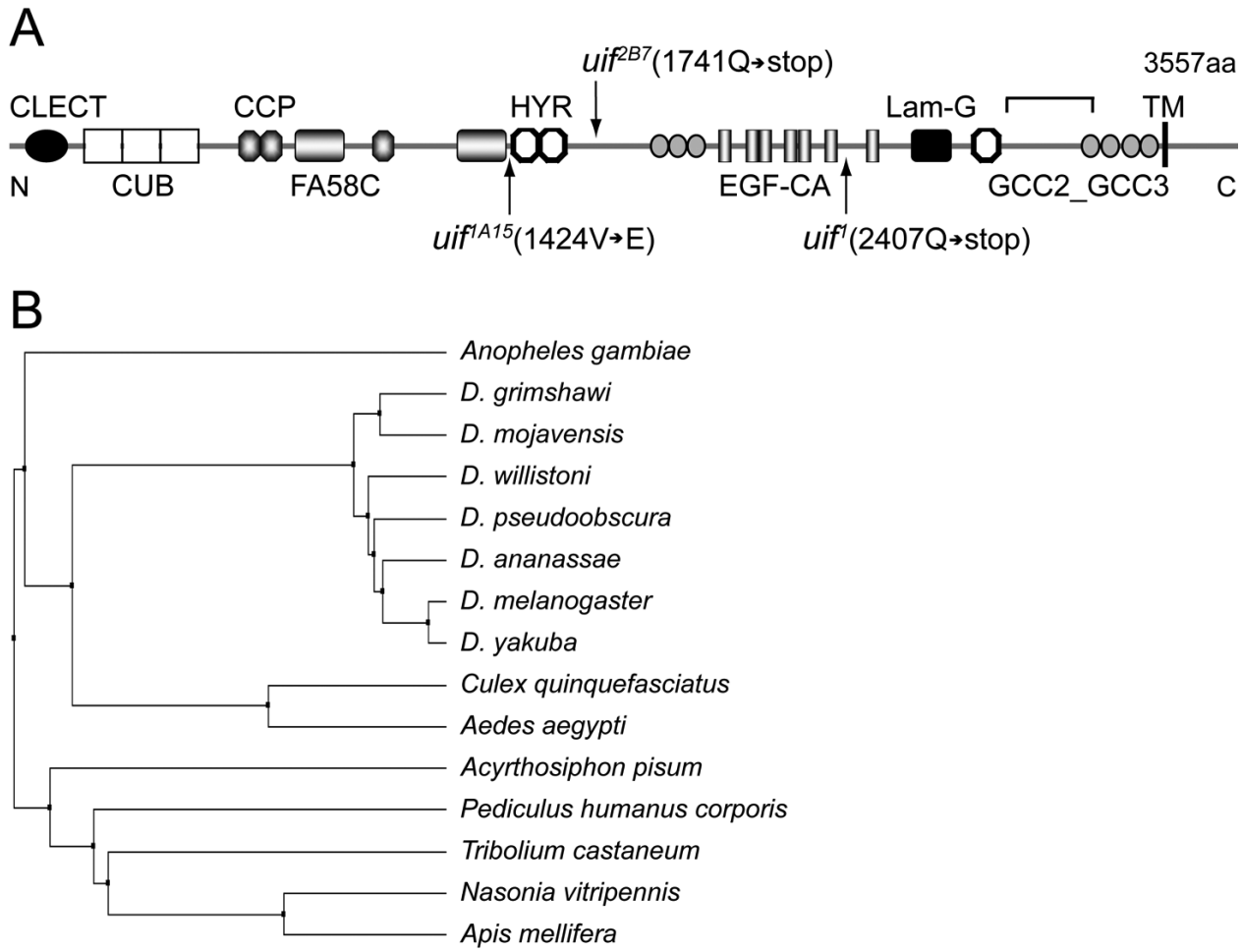

Fig. 1. Molecular organization and conservation of the *uninflatable* gene. (A) Predicted domain organization of Uif protein. A signal sequence is predicted at the N terminus and a single transmembrane (TM) domain is predicted near the C terminus. Molecular details of the mutant alleles are indicated. *uif*^{1} and *uif*^{2B7} result from premature stop codons, whereas *uif*^{1A15} results from a missense mutation changing Val^{1424} into Glu. CLECT, C-type lectin-like domain; CUB, complement C1r/C1s, Uegf, Bmp1 domain; CCP, complement control protein domain; FA58C, coagulation factor 5/8 C-terminal domain; HYR, hyaline repeat domain; EGF-CA, calcium binding Epidermal Growth Factor-like domain; Lam-G, laminin G domain. The region of Uif used for antibody generation is indicated by the bracket above the model. (B) Phylogenetic tree of Uif orthologs based upon full-length protein sequences. The sequence divergence of Uif correlates precisely with the evolutionary relationships found within the insect order, and no Uif homologs could be identified outside this order.

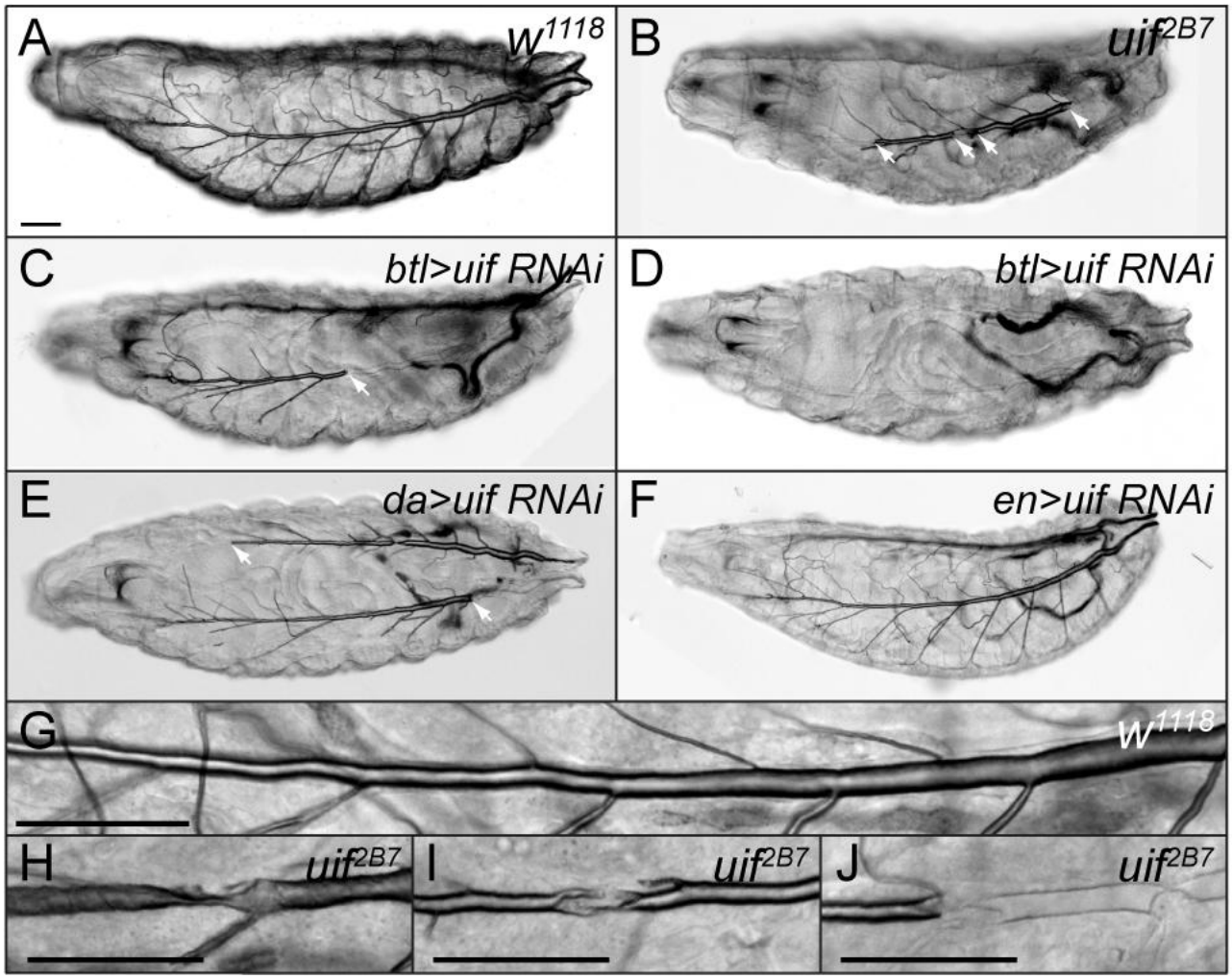

Fig. 2. *uif* mutant first instar larvae have defects in tracheal inflation and damaged tracheal tubes. (A-D) Brightfield photomicrographs of (A)w^{1118}, (B) uif^{2B7}, (C, D) *btl-Gal4/UAS-uifRNAi*, (E) *UAS-uifRNAi/+; da-Gal4/+*, (F) *en-Gal4/UAS-uifRNAi* newly hatched first instar larvae. All animals are depicted with anterior to the left. Refracted light makes the inflated trachea clearly visible in the wild type larva and shows that the tracheae of *uif* mutant animals are partially to completely uninflated. The boundary of inflated/uninflated trachea are marked by arrows in B, C and E. Note that *en>uifRNAi* larvae have normally inflated tracheae (F). (G-J) Differential Interference Contrast micrographs of dorsal tracheal trunks in w^{1118} (G) and uif^{2B7} (H-J) newly hatched first instar larvae. Note the regular diameter of the inflated dorsal trunk in the wild type larva as it gradually tapers towards the anterior over 6 segments, and contrast that to *uif* mutant tracheae that appear twisted or crushed and show discontinuous regions that are uninflated. Scale bars = 50μm.

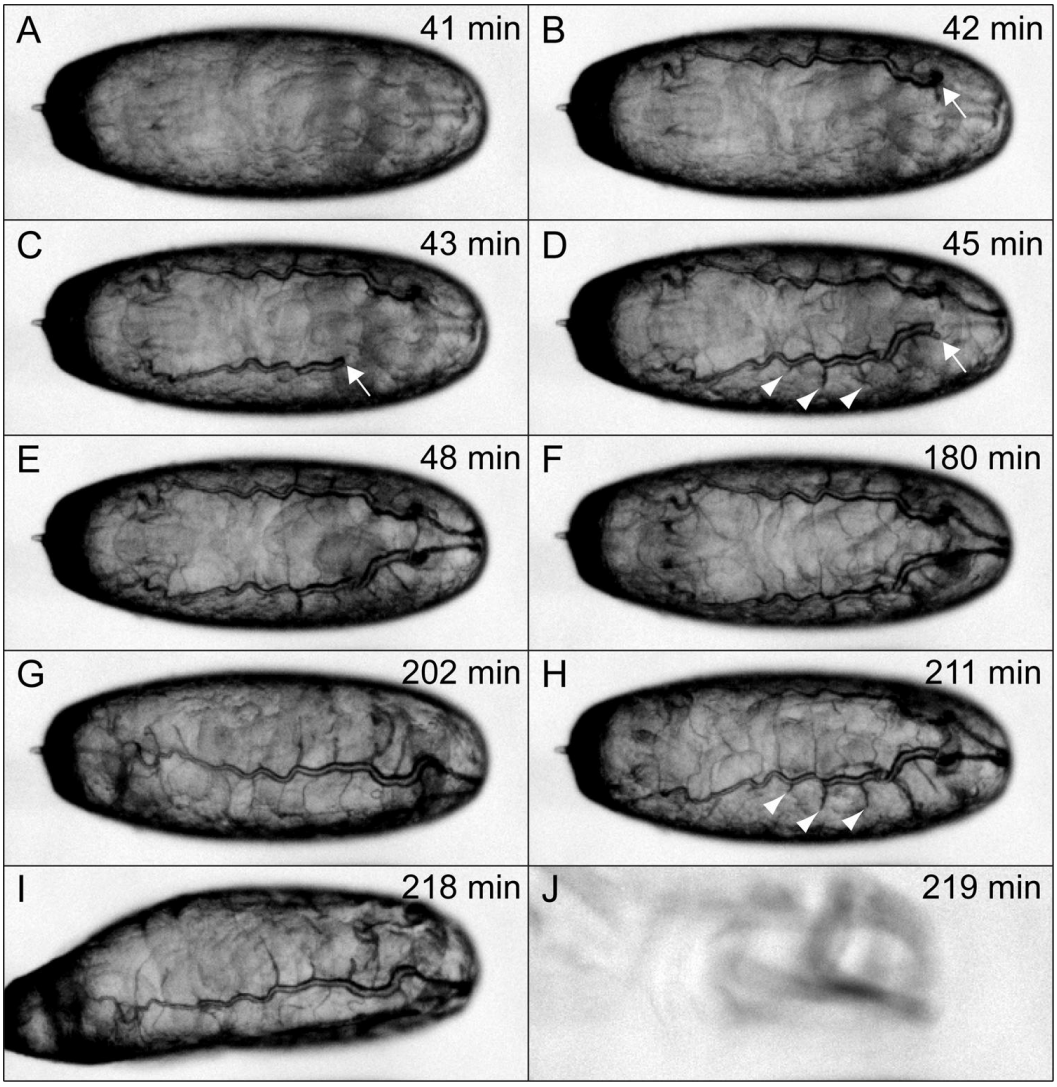

Fig. 3. *uif*^{2B7} mutant animals fail to establish fully inflated tracheae during embryogenesis. Selected brightfield photomicrographs from a time-lapse series of an *uif*^{2B7} mutant embryo showing a rapid period of tracheal inflation (A-E), followed by more than two hours with no additional inflation (F-I). Times given are relative to the start of observation which occurred in mid stage 17 of embryogenesis. The full time series can be seen in Supplemental movie1. Note that the inflation phase lasts for seven minutes and results in fully inflated dorsal trunks with little inflation distal to the transverse connectives in each metamere. Arrows indicate the extent of inflation of the dorsal trunk during the initial inflation phase. Arrowheads in D and H indicate the extent of inflation in three adjacent metameres and show that there is no additional inflation of these segments over a 166 minute period. Even though the animal has not completed tracheal inflation, it hatches and crawls away (J).

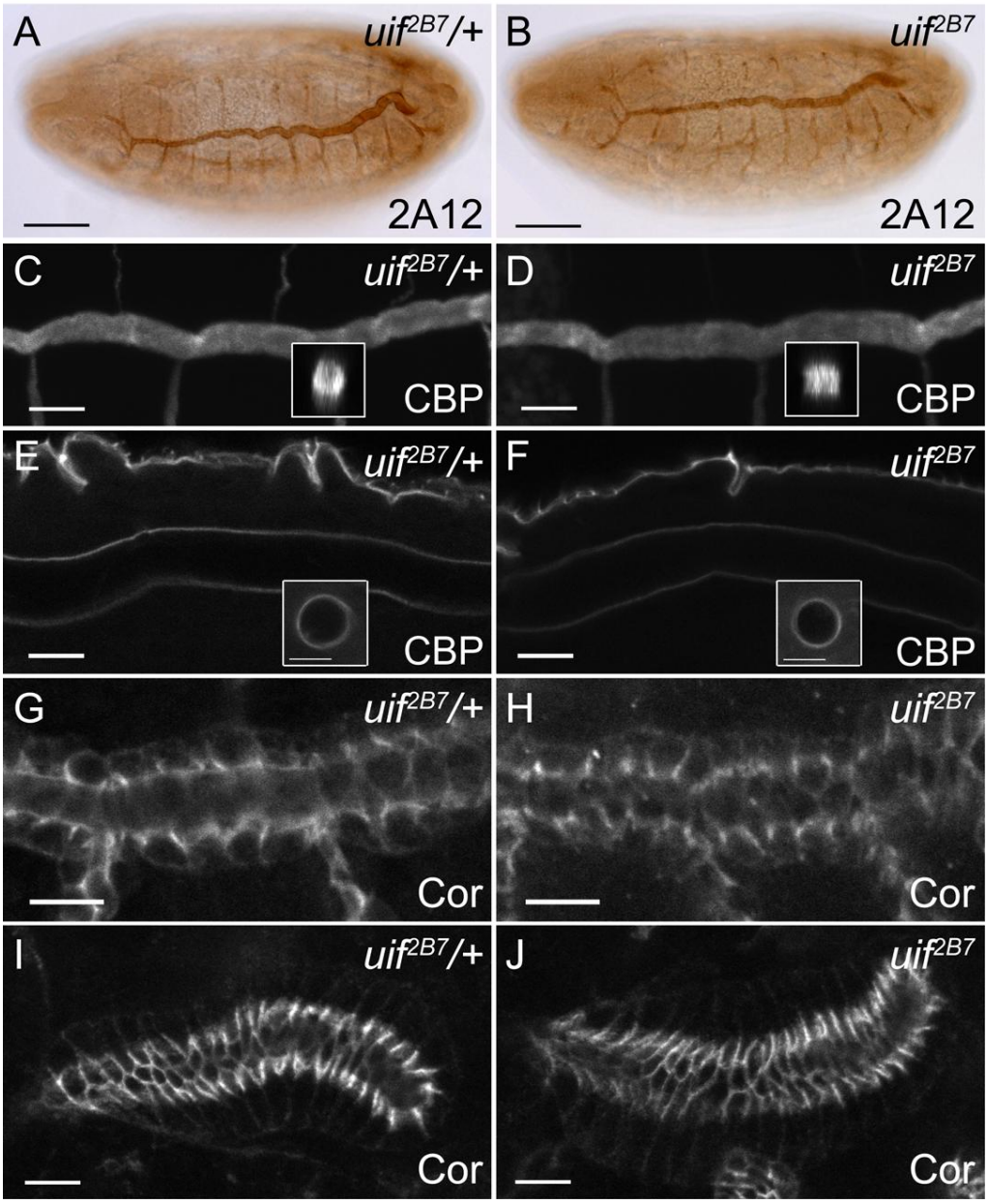

Fig. 4. *uif* mutant embryos have normal tracheal patterning and maturation, and have intact septate junctions. (A, B) 2A12 staining of stage16 uif^{2B7}/+ and uif^{2B7} embryos demonstrates that tracheal patterning as well as dorsal trunk tube length and diameter are normal in *uif* mutants at this stage of development. (C-F) Confocal optical sections of uif^{2B7}/+ and uif^{2B7} embryos stained with chitin binding probe (CBP) show a continuous chitin cable in the lumens of wild type and *uif* mutant animals at stage 16 (insets in C and D show xz projections of the dorsal trucks) that is completely cleared by mid-stage 17 (insets in E and F show optical cross sections of the dorsal trunk that can be visualized near the posterior of the animals). Note that CBP staining still outlines the apical surface of the dorsal trunk in mid-stage 17 mutant embryos indicating the presence of a chitinous cuticle. (G-J) uif^{2B7}/+ and uif^{2B7} embryos stained with antibodies against the septate junction protein Coracle (Cor) show the correct localization of this protein in an *uif* mutant trachea (H) and salivary gland (J). In all panels, anterior is to the left. Scale bars = 50μm in A-B; 10μm in C-J.

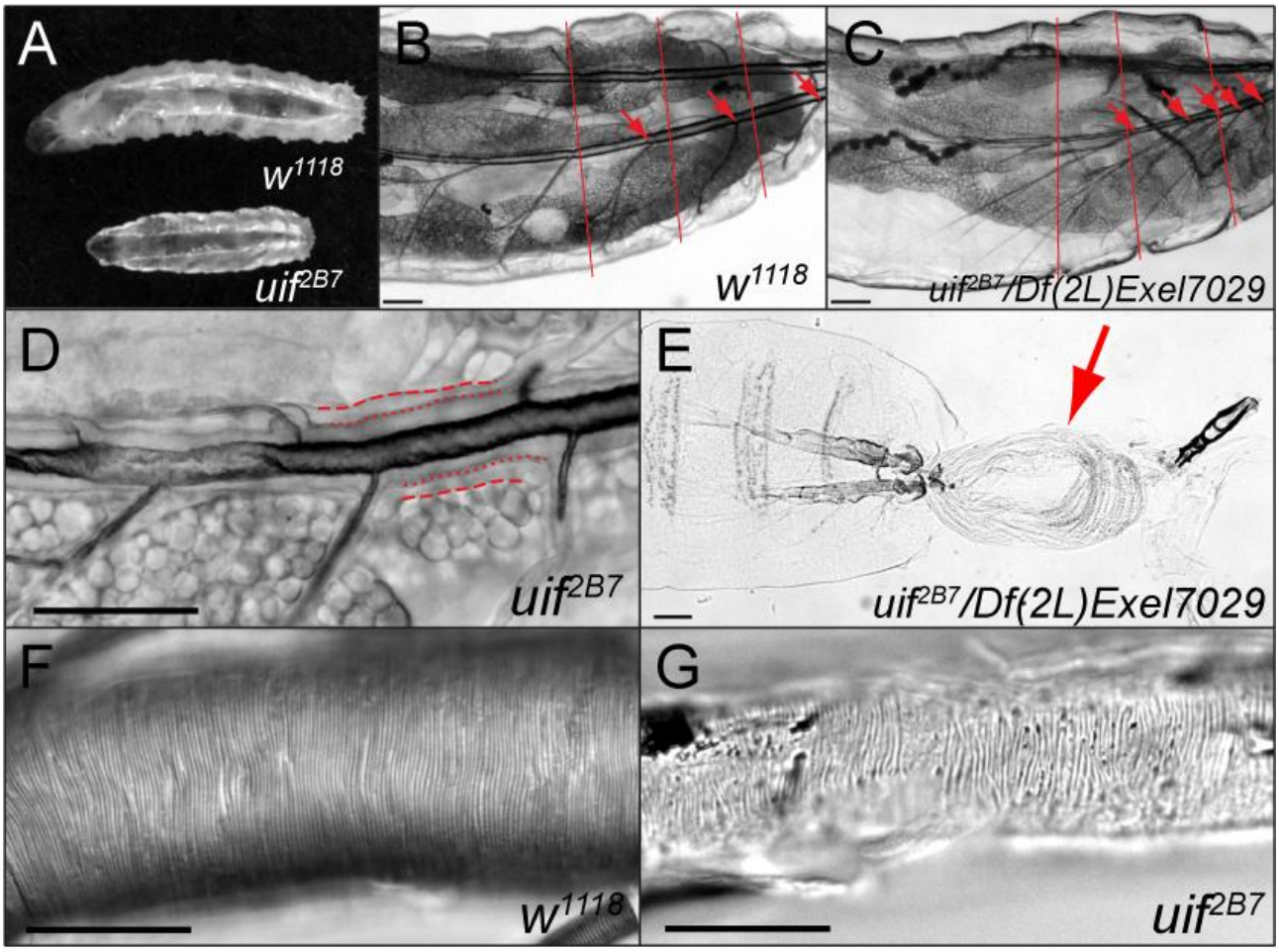

Fig. 5. *uif* mutant second and third instar larvae have tracheal growth and molting defects. (A) Brightfield photomicrograph of a 5-day-old w^{1118} 3rd instar larva and a 5-day-old uif^{2B7} 3rd instar larva. Note the smaller overall size of the uif^{2B7} mutant larva. (B, C) Brightfield photomicrograph of a w^{1118} 2nd instar larva and a similarly sized $uif^{2B7}/Df(2L)Exel7029$ 3rd instar larva showing a tracheal growth defect in the *uif* mutant larva. Red lines indicate the relative boundaries of the body segments, whereas red arrows indicate the junction of the transverse connective (TC) branch along the dorsal trunk in each metamere. Note that in the wild type larva one TC emanates from each dorsal trunk in each body segment, whereas in the *uif* mutant larva five TCs emanate from the dorsal trunk in the final two body segments. Also note that the *uif* mutant larva has less fat than the w^{1118} larva. (D) *uif* mutant larvae frequently fail to molt their tracheal cuticle. In this 5-day-old uif^{2B7} mutant 2nd instar larva the dashed lines indicate the basal membrane of the tracheal cells, whereas the dotted lines indicate the apical surface of the tracheal cells. Note the presence of two layers of cuticle with only the inner or 1st instar lumen being inflated. (E) $uif^{2B7}/Df(2L)Exel7029$ mutant 3rd instar larva that has failed to complete its molt. The previous epidermal cuticle (arrow) is connected at the posterior spiracles. (F, G) DIC photomicrographs of w^{1118} and uif^{2B7} 3rd instar larval posterior dorsal tracheal trunks. Note the regular pattern of the taenidial folds in the wild type trachea. Although the trachea in G is uninflated, taenidia are present and are organized into roughly parallel rows that run perpendicular to the long axis of the trachea. Scale bars = 100μm in B, C and E; 50μm in D, F and G.

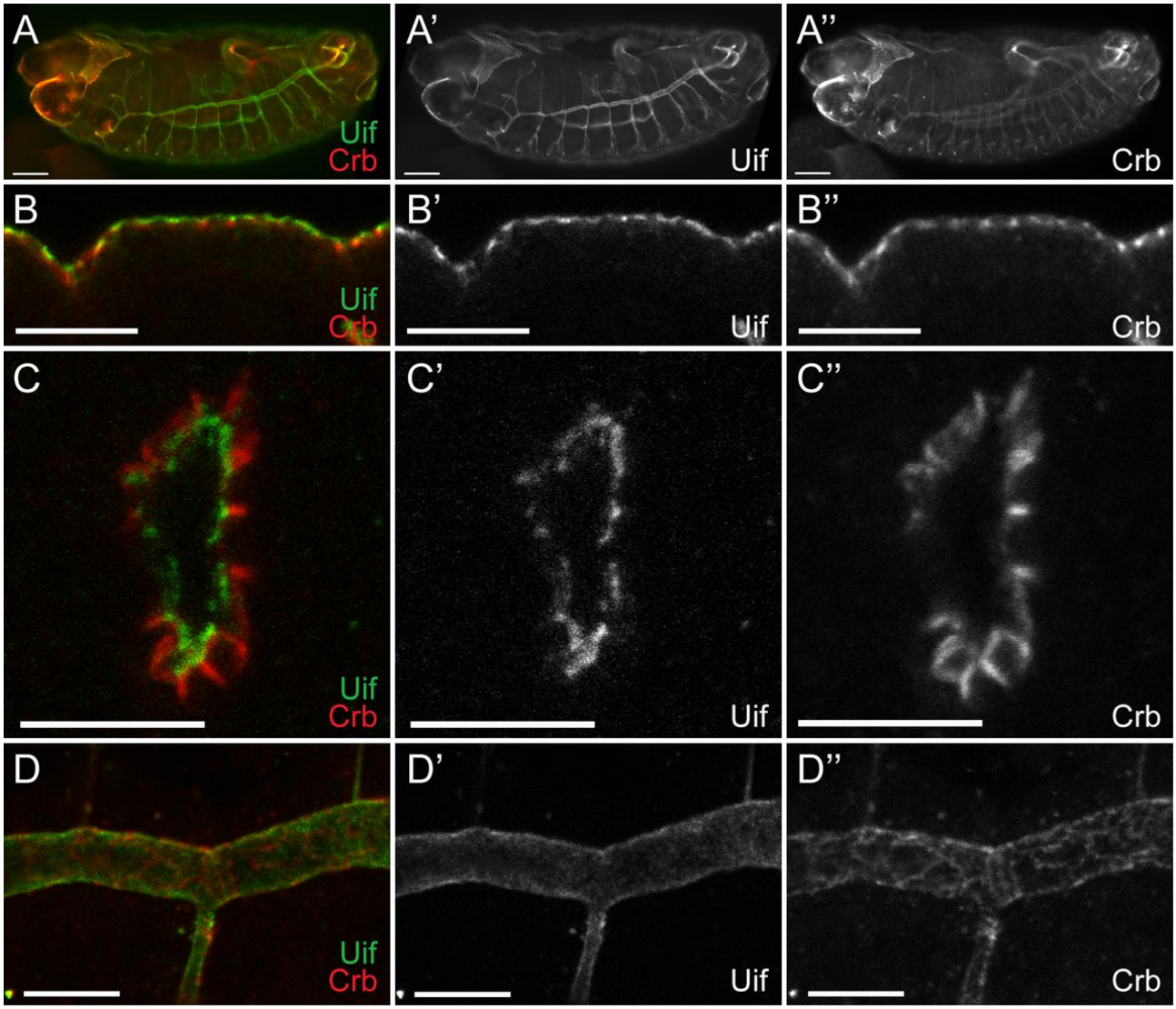

Fig. 6. Uif is expressed on the apical plasma membrane of ectodermally derived epithelial cells during embryogenesis. (A) Open pinhole confocal micrograph of a stage 15 w^{1118} embryo double labeled with anti-Uif (green) and anti-Crb (red) antibodies. Individual channels are shown for Uif (A') and Crb (A''). Uif expression can be detected in the fore- and hindgut, the epidermis and most strongly in the tracheal system. (B-D) Higher magnification confocal optical sections of w^{1118} embryos stained with anti-Uif (green) and anti-Crb (red) antibodies. Individual channels are shown for Uif (') and Crb (''). Tissues include the epidermis at stage 14 (B-B"), the tracheal placode at stage 11 (C-C"), and the tracheal dorsal trunk at stage 14 (D-D"). Note that Uif is expressed in a domain that is more apical than Crbs in all of these tissues. In all cases anterior is to the left. In panel B apical is up. In panel C apical is to the center of the placode. Scale bars = 50μm in A; 10μm in B-D.